

RESEARCH ARTICLE

10.1002/2016JB012919

Key Points:

- New 3-D shear wave velocity model computed from ambient noise cross correlations offshore Southern California
- Model reflects the transition from continental to oceanic lithosphere in a region with complex tectonic history
- Deeper lithosphere controlled by isostatic compensation, with no indication in model of an ancient Farallon slab

Supporting Information:

- Supporting Information S1

Correspondence to:

D. C. Bowden,
dbowden@caltech.edu

Citation:

Bowden, D. C., M. D. Kohler, V. C. Tsai, and D. S. Weeraratne (2016), Offshore Southern California lithospheric velocity structure from noise cross-correlation functions, *J. Geophys. Res. Solid Earth*, 121, doi:10.1002/2016JB012919.

Received 16 FEB 2016

Accepted 17 APR 2016

Accepted article online 20 APR 2016

Offshore Southern California lithospheric velocity structure from noise cross-correlation functions

D. C. Bowden¹, M. D. Kohler², V. C. Tsai¹, and D. S. Weeraratne³

¹Seismological Laboratory, California Institute of Technology, Pasadena, California, USA, ²Department of Mechanical and Civil Engineering, California Institute of Technology, Pasadena, California, USA, ³California State University, Northridge, California, USA

Abstract A new shear wave velocity model offshore Southern California is presented that images plate boundary deformation including both thickening and thinning of the crustal and mantle lithosphere at the westernmost edge of the North American continent. The Asthenospheric and Lithospheric Broadband Architecture from the California Offshore Region Experiment (ALBACORE) ocean bottom seismometer array, together with 65 stations of the onshore Southern California Seismic Network, is used to measure ambient noise correlation functions and Rayleigh wave dispersion curves which are inverted for 3-D shear wave velocities. The resulting velocity model defines the transition from continental lithosphere to oceanic, illuminating the complex history and deformation in the region. A transition to the present-day strike-slip regime between the Pacific and North American Plates resulted in broad deformation and capture of the now >200 km wide continental shelf. Our velocity model suggests the persistence of the uppermost mantle volcanic processes associated with East Pacific Rise spreading adjacent to the Patton Escarpment, which marks the former subduction of Farallon Plate underneath North America. The most prominent of these seismic structures is a low-velocity anomaly underlying the San Juan Seamount, suggesting ponding of magma at the base of the crust, resulting in thickening and ongoing adjustment of the lithosphere due to the localized loading. The velocity model also provides a robust framework for future earthquake location determinations and ground-shaking simulations for risk estimates.

1. Introduction

The tectonically active region of Southern California and the Pacific-North American Plate boundary extends far west of the coastline, but seismic velocity models of the lithosphere and upper mantle in this offshore region are not well developed (from the Continental Borderland to west of the Patton Escarpment, Figure 1), especially at subcrustal depths. This 200 km wide offshore region represents the transition from continental lithosphere to oceanic but is much wider than typical continental shelves and has experienced a significant amount of previous and ongoing deformation as a result of its complex history. Ancient subduction of the Farallon Plate under the North American Plate and the subsequent transition to the current transpressional environment between the Pacific and North American plates have left a wide region with a history of rotation, extension, strike-slip motion, and compression [Crowell, 1968; Atwater, 1970; Atwater, 1989; Dokka, 1989; Stock and Hodges, 1989; Tennyson, 1989; Luyendyk, 1991; Wright, 1991; Crouch and Suppe, 1993; Feigl et al., 1993; Shen et al., 1996; Walls et al., 1998].

An array of 34 ocean bottom seismometers (OBSs) was deployed in 2010 to better understand the Pacific-North American Plate boundary deformational history and to image the region's deeper lithospheric structure. This array was part of the ALBACORE (Asthenospheric and Lithospheric Broadband Architecture from the California Offshore Region Experiment) project [Kohler et al., 2010, 2011]. The OBSs were purposely deployed far west of the coastline and the Patton Escarpment to fully capture the seismic structure transition between continental and oceanic tectonic environments. Local seismicity and multibeam bathymetry data collected during the cruise were used by Legg et al. [2015] to image transpressional fault zones in the Borderland to better constrain seismic risk from offshore faults.

In addition to understanding the tectonic history of the offshore region, there is also a need for accurate seismic velocity models due to its proximity to the San Andreas Fault system. Legg et al. [2015] and others observe a number of seismogenic fault zones in the area, as slip on the Pacific-North American Plate boundary is broadly distributed across Southern California. The Southern California Earthquake Center (SCEC) has compiled

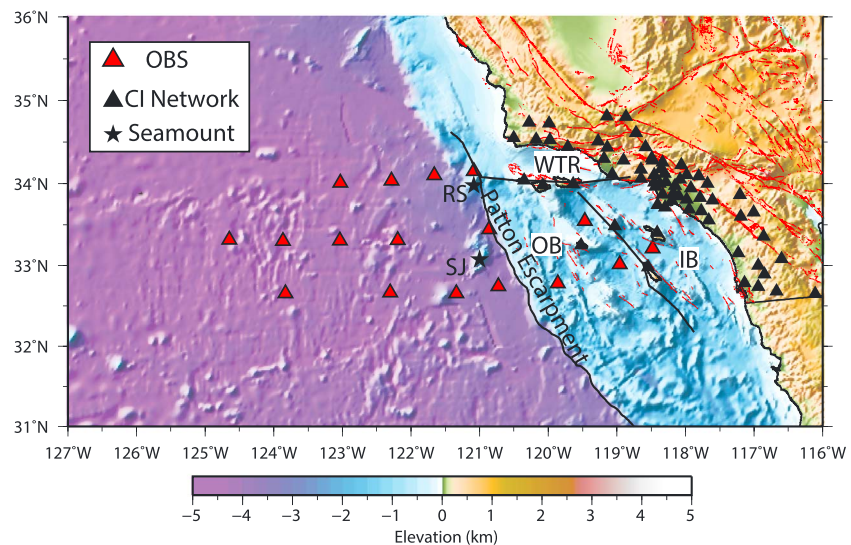


Figure 1. Map of the Southern California offshore region. Triangles indicate broadband seismometers used in the study. The original ALBACORE data set included more stations than indicated (and was roughly on a regular grid), but some stations were not recovered or had technical problems. Tectonic domains indicated include the following: OB: Outer Borderland, IB: Inner Borderland, WTR: Western Transverse Ranges. Seamounts indicated include the following: RS: Rodriguez Seamount; SJ: San Juan Seamount. Black lines separating these regions are inferred from geological structures [Legg *et al.*, 2015].

Community Velocity Models (CVMs) [e.g., Shaw *et al.*, 2015], with the purpose of providing a reliable base for ground motion simulations, earthquake location studies, and deeper tomography. The models are well developed on land and in the populated regions of Los Angeles, but they either end abruptly just off the coastline or they consist of an overly smooth 1-D velocity profile in the offshore region.

This study uses ambient noise tomography to develop a full 3-D velocity model of the region. Based on the array aperture and station spacing, we image the crust and uppermost mantle, from the oceanic lithosphere far west of the Patton Escarpment through the Inner and Outer Borderland and through continental Southern California. A number of studies have demonstrated the efficacy of ambient noise studies to recover velocity models in ocean environments, including Lin *et al.* [2006] across the Pacific Ocean, Harmon *et al.* [2007] and Yao *et al.* [2011] on different arrays near the East Pacific Rise, and Gao and Shen [2015] over the Cascadia Subduction Zone. In nearly all cases, such studies have filled a much needed gap between the near-surface resolution provided by active-source seismic reflection surveys and deeper earthquake-based body wave and surface wave tomography. Ocean environments tend to be noisy due to interactions between the solid earth and the water column, but ambient noise signals are recoverable at shorter periods (i.e., 5–10 s) compared to earthquake surface waves.

2. Tectonic Background

The history and near-surface geology of the California Borderland region have been well documented. Atwater and Stock [1998], for example, provide plate motion reconstructions based on paleomagnetic data, fault structures, and drill core dates and describe how the Western Transverse Ranges block in the northern part of the region was captured by the Pacific Plate and rotated clockwise more than 90° to its current location. This rotation and subsequent strike-slip tectonics of the remaining Borderland have left a series of NW trending faults and basins [Legg, 1991; Crouch and Suppe, 1993], with significant lithospheric thinning under the inner (eastern) part and westward translation of the outer region [Nicholson *et al.*, 1994]. The boundary between the Inner and Outer Borderland is marked by the East Santa Cruz Basin Fault and represents a geologic shift from exhumed Catalina Schist Belt to sediments of the Patton Accretionary Complex [Vedder *et al.*, 1974].

Gravity and seismic profiles provide constraints on upper crustal and sedimentary structure, such as those collected during the Los Angeles Region Seismic Experiment (LARSE) in 1994 [Fuis *et al.*, 2003, 2012] and several lines collected by the U.S. Geological Survey (USGS) in 1978, 1979, and 1990. Inversions of gravity profiles [Miller, 2002; Romanyuk *et al.*, 2007] suggest thinning in the region during periods of extension and subsequent

infiltration of mafic melt in the crust. Similarly, *Weigand* [1994] and *ten Brink et al.*, 2000 use petrological and seismic reflection data to propose that very little mantle lithosphere exists below the Inner Borderland.

Despite the extension and thinning, however, it is not until west of the Patton Escarpment at least 200 km west of the coastline that the geology, bathymetry, and gravity are indicative of normal oceanic lithosphere. The Patton Escarpment is delineated by a cessation of magnetic anomalies typical of oceanic environments [Atwater, 1989], as well as an abrupt change of bathymetry from ~4 km to the west to ~2 km to the east. However, the subsurface structure of the transition is not well imaged, even though it represents the now extinct subduction zone where the Farallon Plate subducted under the North American Plate [Atwater, 1989; Lonsdale, 1991].

Teleseismic earthquakes have been investigated by *Reeves et al.* [2015], from both the ALBACORE array and the permanent Southern California Seismic Network (SCSN), to measure receiver functions in order to image velocity transitions in the region. Their observations provide some of the first direct constraints on depths of the Moho and lithosphere-asthenosphere boundary below the Borderland, as well as general lithospheric structure west of the Patton Escarpment. In agreement with previous studies, they find substantial thinning in the Inner Borderland consistent with extension to accommodate rotation of the Western Transverse Ranges and that the effect of this thinning on deeper lithospheric structure may be even more severe than previously speculated.

3. Data and Methods

Approximately one year of continuous data are used to measure ambient noise cross correlations, using data from 17 broadband ALBACORE OBS stations and 65 on-land SCSN stations (Figure 1). Several of the deployed OBS stations were either not recovered or contained incomplete data. Of the 34 OBSs deployed, 24 of those were broadband and 17 of those were recovered with useful data [Kohler et al., 2011]. All OBS stations used provided three components of seismic data, as well as a differential water pressure gauge (DPG) channel. In this study, only vertical component data are used for the Rayleigh wave observations. The DPG and horizontal components are used only to improve the vertical component signals, as described below. This section describes our signal preprocessing and dispersion curve measurement approach, the linear inversion for slowness at each period, and finally, 1-D depth inversions beneath each grid point to construct the full 3-D tomographic model.

3.1. Signal Preprocessing and Cross Correlation

Underwater environments are generally very noisy due to the action of interfering swells at the surface and ocean currents at depth [Webb, 1998], and such data usually warrant additional preprocessing for ambient noise studies. While the action of water waves and subsequent pressure perturbations on the seafloor is understood to be the dominant source of ambient noise energy in the primary microseism band [Longuet-Higgins, 1950; Gimbert and Tsai, 2015], these sources are relatively well distributed in space and time across the Earth's oceans. The effect of these forces acting directly on a single OBS, however, creates an incoherent (inelastic) signal detrimental to recovering noise correlations. Fortunately, these forces from the water column are also measured by the colocated ALBACORE DPGs (differential pressure gauge), so a transfer function between the two components can be used to remove the unwanted signals [Webb and Crawford, 1999]. Similarly, ocean currents moving past the OBS tilt the seismometer, causing low-frequency noise on the vertical channels that is incoherent with other seismometers in the array. Determining a transfer function with the horizontal components can similarly be used to remove undesired tilt signals [Crawford and Webb, 2000].

We follow the procedure of *Webb and Crawford* [1999] and *Crawford and Webb* [2000] to perform tilt corrections and DPG corrections, and note that a more thorough study of such techniques is described by *Bell et al.* [2015]. These types of corrections are traditionally applied to longer-period signals (i.e., greater than 50 s) than those of this study, but we find that they improve some of our measurements nonetheless. For a given nonvertical component (either horizontal or the DPG), a transfer function to the vertical component is determined from a 12 h period of time known to be quiet and free of earthquakes. This transfer function describes the frequencies and associated phases at which signals are coherent and can be used to predict the signal that a given pressure signal or tilt event will contribute to the vertical component OBS channel. The coherencies vary strongly with location and water depth, so we taper the transfer function to zero outside the period range of 5 to 15 s where the signals are most coherent. We apply all corrections in sequential steps. We first determine and apply a transfer function from one horizontal component to all other components before proceeding. Next, transfer functions from the second horizontal component are applied to both the pressure gauge and vertical

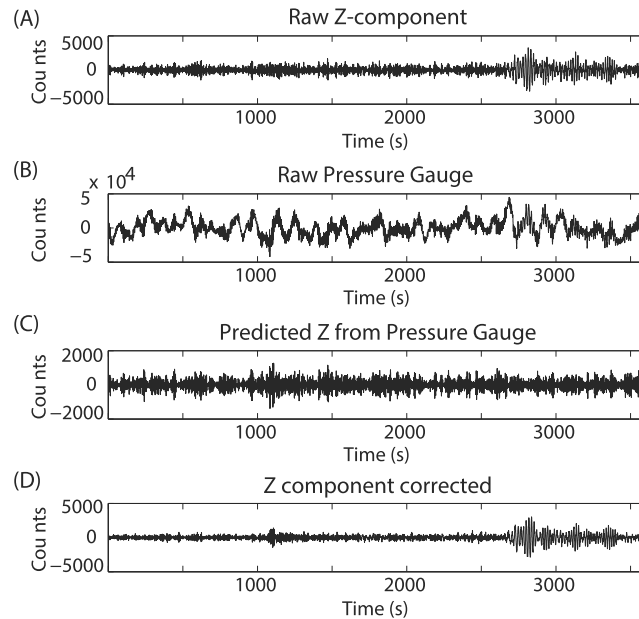


Figure 2. Steps for processing tilt and DPG corrections. (a) An hour of uncorrected vertical component data are presented. The (b) pressure gauge component is used to predict an effect on the (c) vertical component which is subtracted from the raw vertical (Figure 2a) to produce a (d) cleaned time series.

component, and finally, we apply the transfer function from pressure gauge to vertical. This sequential processing (i.e., also correcting one horizontal based on the other) ensures that any effect of the water column which affects both components coherently will not be mistakenly corrected twice. We also note that the transfer function is independent of units, so we do not apply the vertical instrument response until after the entire process is complete.

The effects of the wave loading and tilt corrections are often dramatic and potentially useful for event detection (Figure 2d). In contrast, we find that for the 5–9 s period range of noise cross correlations, the application of the corrections reduces the strength of the fundamental surface mode observation relative to the first overtone. Indeed, this is likely why the original work of Webb and Crawford only uses the technique at longer periods. It is likely that at the shorter periods our fundamental

mode measurements are so sensitive to the water layer that removing signals coherent with the DPG and tilt also removes much of the useful signal. The first overtone, however, is sensitive to deeper structure and is relatively easier to measure with the correction. Thus, we consider both the uncorrected and corrected sets of noise correlations when measuring dispersion curves (Figures 3 and 4), using whichever set shows a stronger signal at a given period.

Before performing the ambient noise cross correlations, we also apply standard time domain normalization and spectral whitening as described by *Bensen et al.* [2007]. These techniques help suppress the effects of earthquakes and other nonstationary sources of energy which may bias the noise correlation function (NCF). We take the symmetric component of the NCF by summing the data from positive and negative correlation time lags. We stack the entire year of data to help ensure that we have averaged out any azimuthal bias by seasonal weather patterns, even though we find that the NCFs are generally stable with three to five months of stacking.

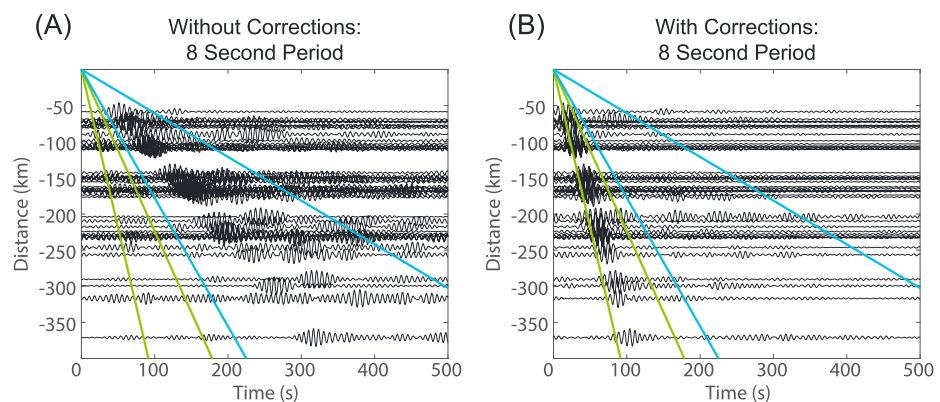


Figure 3. Record section of station pairs in the deep ocean. (a) Raw data. (b) Data corrected for tilt and pressure loading. We observe a significant difference in our ability to observe the fundamental mode and first overtone, with expected ranges of velocities for both modes windowed in blue and green, respectively.

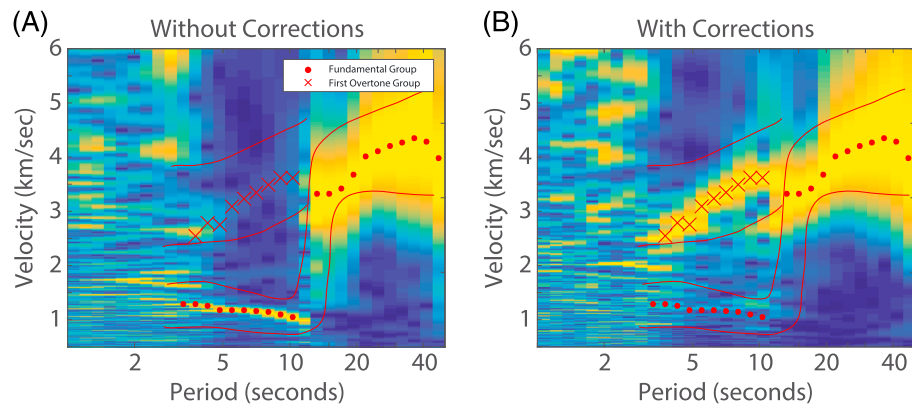


Figure 4. An example of extracting dispersion data from a single NCF. Each column represents a narrow band-pass filter, where the color represents a normalized amplitude of the signal envelope. Red lines bound the expected range of measurements for the oceanic region, for both the fundamental mode (lower set of curves) and first overtone (higher set). Red dots and X's indicate selected group velocity measurements, again from both corrected and uncorrected data.

Measuring dispersion from the NCFs proved challenging, however, as the extremely varied tectonic nature of the region, and varying water depths meant that often the arrival of a given mode could not be cleanly identified with a purely automated script. Velocity changes created spurious reflections and scatterers in the NCFs especially in the transition region between the Borderland and coastline. Approximately half the dispersion curves were manually picked prior to application of an automated frequency-time analysis procedure (FTAN), based on the script of *Levshin and Ritzwoller* [2001]. While the original script allowed for setting a single maximum and minimum velocity, our modification considers a predetermined reference dispersion curve (determined from manual observation of a subset of the NCFs) and searches for the maximum within given bounds, effectively guiding the automated search more precisely as a function of period (red lines in Figure 4). Four additional quality control checks are employed: a signal-to-noise ratio (SNR) test, removal of data more than two standard deviations from the average at each period, removal of rays with distances less than 2 times the expected wavelength, and lastly, a manual examination of all dispersion curves with manual removal of any curves which appear biased by some other reflection or complication. The signal-to-noise ratio is defined as the peak group amplitude divided by the root-mean-square of signals outside the expected arrival window, where measurements with $SNR < 3$ were rejected (and the SNR was later used again to weight raypaths in the inversion). Table 1 describes the number of raypaths retained out of the possible 3321 station pairs, and examples of their spatial distributions are shown later when the inversion process is described.

Figures 5a–5c show samples of resulting dispersion measurements, grouped by pairs within distinct geologic regions. The station pairs in deeper water (Figure 5a) are in approximately constant 4 km water depth and are located on the relatively homogeneous abyssal plain; thus, they are clean enough to distinguish the first overtone. This is particularly useful since the fundamental mode in the period range 5–10 s is dominated by the water layer (with phase velocities close to 1 km/s), while the higher modes have sensitivity primarily to crustal structure. Also, there is a gap in measurements around 10 s (Figure 5a), which represents a transition from sensitivity predominantly to the water layer to sensitivity to the uppermost crust. Our band-pass filters are Gaussian functions with finite width; thus, at a period of around 10 s, signals are dominated by both sensitivities' velocity and period. Figures 5b and 5c represent raypaths in the Borderland and on land and show significantly more scatter due to tectonic heterogeneity.

3.2. Inversion for 2-D Maps at Each Period

The first step toward constructing a 3-D shear wave velocity model consisted of inverting the raypaths at 20 different periods for a 2-D grid of phase and group velocity measurements, following the least squares

Table 1. Number of Raypaths Used in Each 2D Inversion, at a Range of Representative Periods								
Period (s)	5	7.5	10	15	20	30	40	50
No. of Raypaths (Fundamental Mode)	934	1257	1357	1263	1114	996	839	49
No. of Raypaths (First Overtone)	43	53	8	-	-	-	-	-

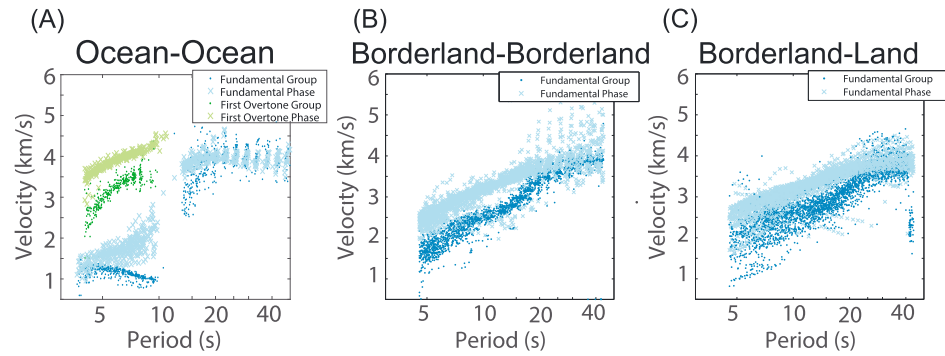


Figure 5. Sample dispersion curves grouped by dominant structural features. Raypaths not included in these figures span multiple geologic domains, such as from the deep ocean to inland, and such raypaths show more variability than those presented here.

approach of *Barmin et al.* [2001] and *Ma and Clayton* [2014]. Group and phase measurements are determined at each period for both fundamental and first overtone data (e.g., Figure 5). Velocities are described by a deviation in slowness from the average, providing a linearized inverse problem

$$\Delta t_i = \int \frac{m_i}{c_0} ds, \leftrightarrow d = Gm$$

where $m_i = (c_0 - c)/c$.

$$m = (G'WG + \beta L1'L1 + \alpha F'F)^{-1} G'Wd$$

F describes a small amount of Gaussian smoothing applied to each ray such that it sufficiently approximates the true finite-frequency kernel given the relatively course grid spacing [*Barmin et al.*, 2001]. $L1$ describes a Tikhonov regularization [*Loris et al.*, 2007], which reduces the first derivative across the inverted grid, and stabilizes grid points that are outside our region of densest rays. W is a diagonal matrix of SNR used to weight better station pairs; specifically, the diagonal elements are the normalized log of $1/\text{SNR}$ to prevent overweighting. The amount of regularization is manually tuned to provide images which are smooth on the length scale of our station spacing but with as little smoothing as possible so that the dynamic range of velocities is optimally maximized. While the conversion to slowness and the formulation of the inverse problem are linear, regularization and smoothing do not have a linear effect on the recovered velocities; however, checkerboard tests indicate that this effect is minimal for our range of velocities. Figure 6 shows an example of input rays and resulting 2-D model at a 5 s period, and additional periods (12 s, 20 s, and 40 s) can be found in Figures S1–S3 in the supporting information.

Figure 7 shows a checkerboard test with the resulting inversion results using the raypath data set corresponding to 8.5 s period. Figure 7b shows that we successfully recover the majority of features on the length scale of our station spacing. Additional checkerboard tests are presented in the supporting information Figures S1–S3. An additional recovery test designed with a single strong boundary along the Patton Escarpment is shown in the supporting information Text S1. The results from this second test (Figure S4b) indicate that we can resolve features along the Patton Escarpment, specifically, to a lateral length scale of 50 km. Our results are limited to the resolution of our grid spacing, but we find that the presence of a strong boundary does not bias or degrade the slowness inversion accuracy or resolution.

3.3. Inversion for Shear Wave Velocity With Depth

With velocities represented on a set of 2-D grids, the next step toward constructing the shear wave velocity model is to invert the dispersion curves at each grid point for 1-D structure. We use a modal summation technique to compute synthetic dispersion curves and compare to data (using the software package Computer Programs in Seismology [*Herrmann*, 2013]). The inversion is allowed to iterate for each grid point, improving each 1-D profile to minimize the misfit between the dispersion curve data and the synthetic dispersion curves, until the profiles converge. The 1-D shear velocity profiles are defined at 1 km intervals, though a lack of resolution and uniqueness at depth limits the scale of features we can interpret to 5–10 km, described later. We uniquely solve only for shear wave velocities; any relation to compressional wave velocities or density used in the CPS package relies

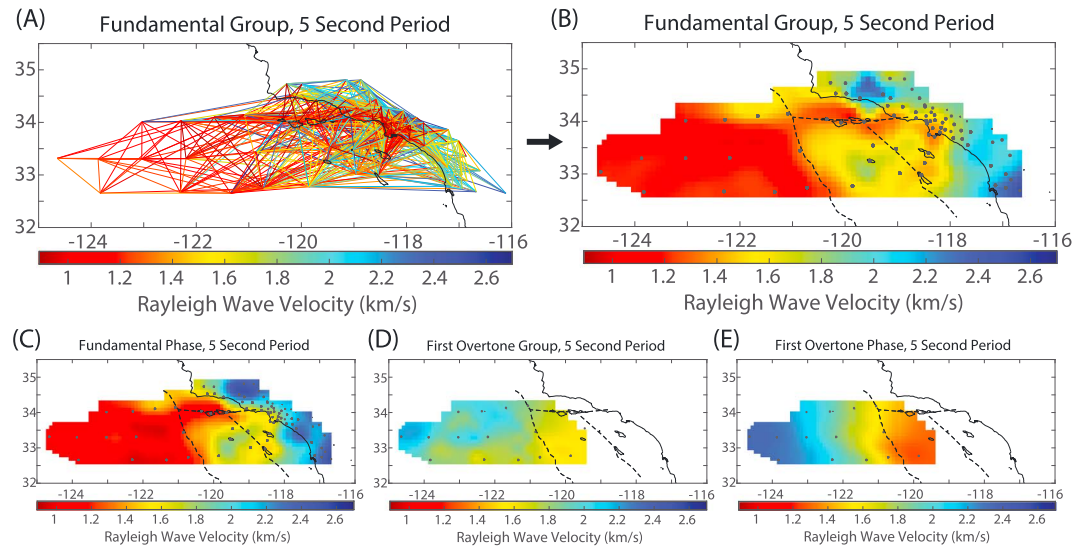


Figure 6. Examples of 2-D grid inversions for a given period. (a) Input rays are inverted on a (b) regular grid. The same procedure is applied to raypath measurements of (c) fundamental phase, (d) first overtone group, and (e) first overtone phase. The grid used for first overtone measurements is smaller to respect the region for which measurements were made. The same procedure is applied for 20 logarithmically spaced periods from 5 to 50 s.

on standard empirical relationships (i.e., V_p/V_s ratio can be approximated as 1.7). To minimize the bias from a chosen starting model, we use a range of 41 input starting models. All of these are linear ramps of increasing velocity or otherwise constant in velocity and linearly stepping between end-member expectations of velocities between 2 km/s and 5 km/s and whose only constraint is a water layer of fixed thickness appropriate for each grid point. We choose to use only simple starting models, as the deeper geologic structure of the region is still relatively unknown and we did not want to incorrectly bias the final model. We average the results from these starting models, though we find that the resulting velocity model is fairly independent of starting model (starting models and example 1-D profiles are shown in the supporting information Figure S5). This final model predicts dispersion data with an average misfit of 0.18 km/s, which is approximately twice as accurate as would be predicted by the synthetic, simple model produced from standard reference profiles described in the supporting information Text S1.

Figure 8 shows the sensitivity kernels for an average, smooth 1-D profile underneath a 4 km thick water layer and shows that the first overtone is considerably more sensitive to shallow crustal structure in this environment. The kernels are calculated by perturbing each layer sequentially by a 1% increase in shear wave speed. The water layer has a shear wave speed of zero, so the kernels' low sensitivity in the water layer is a result of no perturbation in that layer; the extremely low fundamental group and phase measurements in the short-period range are further evidence of the water sensitivity on the kernel (pure water should have a phase velocity of around 1.4 km/s). The stronger sensitivity of the first overtone highlights the importance of including it (where available) in an oceanic environment.

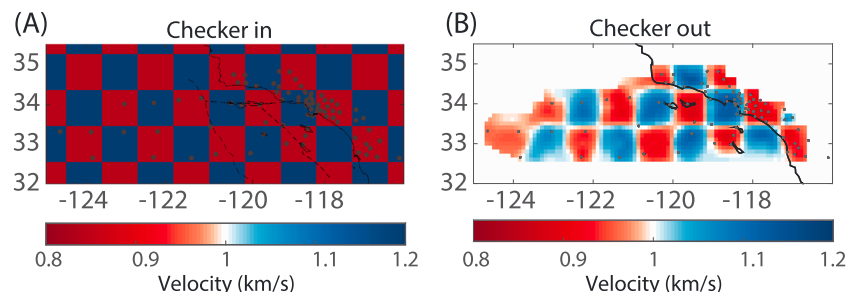


Figure 7. Checkerboard test using raypaths available for fundamental group measurements corresponding to 8.5 s period. We trim all later maps to the region well covered by raypath density and well recovered in such checkerboard tests.

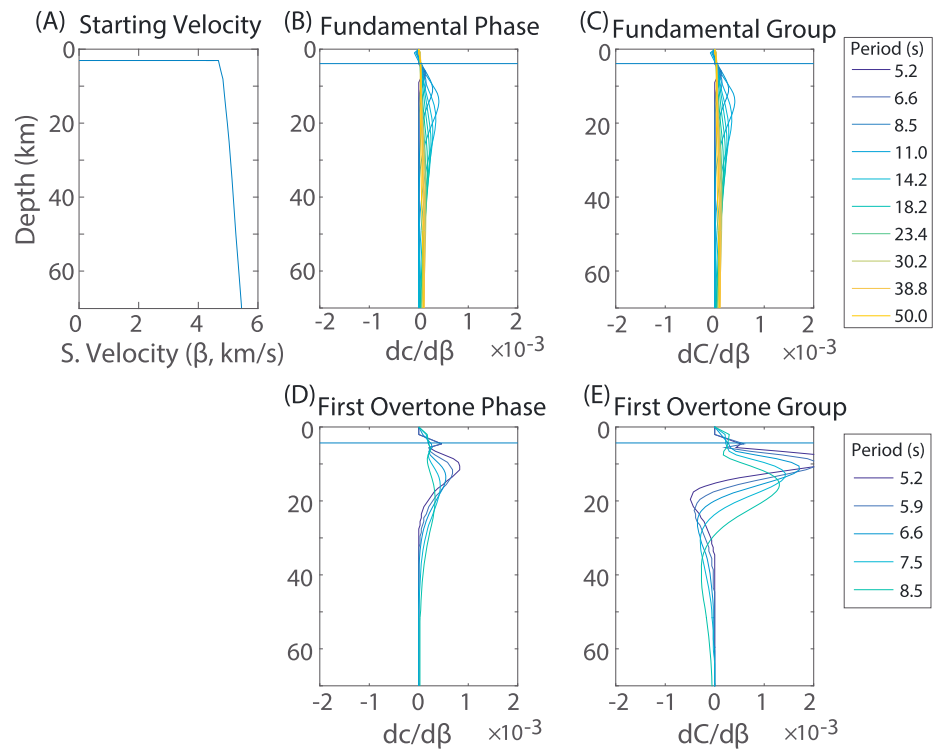


Figure 8. Depth sensitivity kernels using a 4 km thick water layer and an average of our deep water 1-D velocity profiles. (a) The starting model used with a 4 km water depth being the predominant feature. (b and c) Group and phase sensitivities for the fundamental mode. (d and e) Group and phase sensitivities for the first overtone.

As with any inversion of this type, we resolve shallow features better than deeper features. The sensitivity kernels (Figure 8) and final iteration resolution matrices indicate a vertical resolution of 5 km in shallow regions (1–30 km depth), with vertical resolution degrading to ~10 km by 50 km depth. Some of the cross sections presented later include model features down to 70 km depth, though we limit our interpretations of such deeper structures. Using a range of input starting models (described above and in the supporting information Figure S5) does not explicitly indicate resolution of features, but a relatively small standard deviation in output models does provide confidence that the inversion process is stable in converging to the presented model, even at depths of 50 km and greater.

4. Results and Discussion

Final shear wave velocity model results are shown in Figures 9 (plan views at different depths) and 10 (vertical cross sections). We observe that the Borderland region more closely resembles continental crust, with a distinct transition to oceanic structure moving west across the Patton Escarpment. Again, our model resolves lateral variations of roughly 50 km, and the vertical resolution is 5–10 km depending on depth. Our interpretation of the model is focused on a few specific structures, including the depth and shape of the Moho, defined here as the transition from about 3.7 km/s to 4.0 km/s. We also compare the Inner and Outer Borderland regions, consider the existence (or lack thereof) of a remnant subducted slab, and hypothesize about the relatively diffuse, deeper structure underneath the Patton Escarpment and nearby seamounts.

We interpret a deeper Moho (~25 km) under the Western Transverse Ranges (Figure 10a: profile A-A') and crustal thinning in the Outer and Inner Borderland south of the Western Transverse Ranges (Figure 10: B-B', C-C', and D-D'). This is consistent with Western Transverse Ranges capture by the Pacific Plate and subsequent rotation [i.e., *Nicholson et al., 1994*]. We do not observe a crustal root as thick or wide as is observed beneath other continental lithosphere in the region (i.e., the on-land extent of the Transverse Ranges) [*Hadley and Kanamori, 1977; Raikes, 1980; Walck and Minster, 1982; Humphreys and Clayton, 1990; Kohler, 1999*], suggesting at least that some deeper Borderland lithosphere was sheared away in the process of rotation. We observe a small

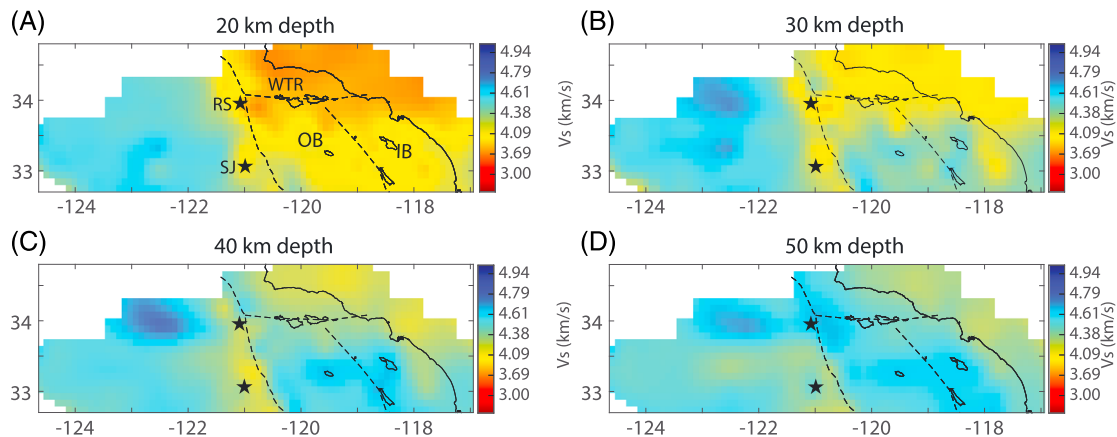


Figure 9. Plan views showing the final shear wave velocity model at depths of (a) 20 km, (b) 30 km, (c) 40 km, and (d) 50 km. Stars indicate the location of the Rodriguez seamount (RS) and San Juan seamount (SJ). Tectonic provinces indicated include the Western Transverse Ranges (WTR), Outer Borderland (OB), and Inner Borderland (IB).

concentration of anomalously thicker shallow crust, approximately 30 km thick by 30 km wide, just east of the Patton Escarpment in A-A' (roughly 310 km along profile) and interpret this to be the result of pinching between the westernmost endpoint of the rotating Western Transverse Ranges block and the northward shifting Outer Borderland. We may be seeing the velocity signature of additional thickening or shearing at the edges of a block which has been rotated more than 90°. The fast anomaly at depths greater than 50 km beneath the Outer Borderland in A-A' (325 km along profile) likely relates to the same processes, as mantle lithosphere is depleted or missing compared to other regions. This fast anomaly would likely be seen underneath other regions if our methodology allowed for deeper observations.

Comparing the Inner and Outer Borderland, we do not observe a significant difference in velocity structure. *Nicholson et al.* [1994] suggest that the Outer Borderland was laterally translated, with the bulk of extension and rotation occurring in the Inner Borderland. While our model does indicate small regions of slightly thinner crust in the Inner Borderland (profile C-C'), the difference is minimal, and we suggest that deeper crust may have subsequently flowed eastward into the Inner Borderland to equilibrate the depths of these structures, analogous to observations from the Basin and Range [Parsons, 1995], where the Moho is observed to be flatter than might be expected underneath the extensional regime [Klemperer et al., 1986].

The seismic velocity model is generally consistent with gravity inversions of the USGS and LARSE lines of *Miller* [2002] and *Romanyuk et al.* [2007], both of which incorporate near-surface seismic reflection data, borehole measurements, and magnetic anomalies. For example, the depth of the Moho and the sloping increase in this depth across the coastline are evident in both models (Figure 10, profile C-C', between horizontal distances of 400 and 450 km). We observe a fast anomaly in the Santa Cruz Basin (Figure 9, profile B-B', at a horizontal distance of 350 km) with a depth of 2–10 km, which *Miller* [2002] interprets as an outcrop of volcanic rocks, consistent with borehole measurements from *Bohannon and Geist* [1998]. Unlike the gravity inversions, however, we observe a lower velocity structure beneath the Santa Cruz Basin to a depth of 50 km, which we interpret as isostatic compensation for the denser shallow material above.

The existence of a remnant, thin, Farallon slab underplating either part of or the entire region is a subject of much debate [e.g., *Bohannon and Parsons*, 1995; *Fuis*, 1998; *ten Brink et al.*, 2000; *Nazareth and Clayton*, 2003; *Romanyuk et al.*, 2007]. We do not observe evidence for such a layer. A remnant slab would be observable as a thin, high-velocity layer at somewhere between 10 and 20 km depths. Even though our method lacks sharp resolution at this depth range, an underplated slab with a strong velocity contrast should still be evident, even if smoothed or blurred in our results. We also generally observe highly variable Moho depths under the Borderland. If any underplated slab exists, it must have been subject to the same deformation, thinning, and isostatic compensation as the rest of the adjacent lithosphere, making it potentially difficult to image by this or any other technique.

The western side of our study region is characterized by fossil spreading center segments, volcanism, and fracture zones associated with the East Pacific Rise (EPR), which stopped spreading approximately 18–20 Ma

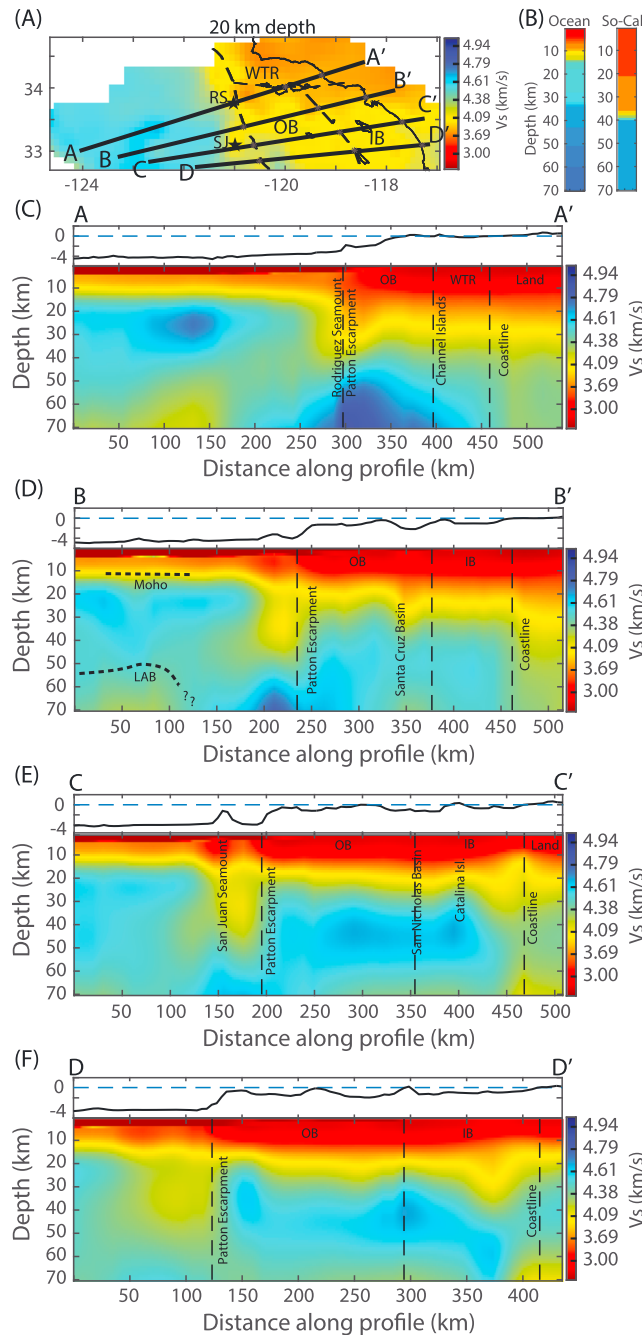


Figure 10. Profiles of the final shear wave velocity model. (a) Dashed lines in the profiles indicate transitions between tectonic domains indicated on the map. (b) Two standard 1-D velocity profiles are provided for reference: a standard oceanic average and a Southern California average [Kohler *et al.*, 2003]. We note that because the ocean model is averaged over all oceanic lithosphere, any lithosphere-asthenosphere boundary is likely averaged out. (c–f) Four cross sections through the 3-D model.

[Atwater, 1989; Lonsdale, 1991]. Two seamounts that resulted from EPR volcanic activity lie within the study region: the San Juan Seamount on the Pacific Plate and the Rodriguez Seamount lying on the continental slope (shown in Figures 1, 9, and 10). Our velocity model suggests the persistence of the uppermost mantle volcanic processes associated with EPR spreading and fracture zones. The most prominent of these seismic structures is a low-velocity anomaly underlying the San Juan Seamount that can be traced throughout each cross section (e.g., Figure 10, C–C' between horizontal distances 150 and 180 km). The low-velocity anomaly is about 30 km wide and has a depth extent of 50 km, well within good resolution limits. Similarly, a low-velocity seismic structure is observed below the Rodriguez Seamount (Figure 9a), but the depth and lateral extent are complicated by the seamount's location at the endpoint of the rotating Transverse Ranges tectonic block [Nicholson *et al.*, 1994]. The San Juan Seamount is part of a chain of nine seamounts with NE-SW orientation off the coast of central and Southern California. The seamounts were once islands that were the product of small-volume volcanic eruptions due to decompression melting of sub-oceanic mantle melts rising along zones of weakness in the oceanic crust [Paduan *et al.*, 2009; Davis *et al.*, 2010]. On the San Juan Seamount there is geochemical evidence for eruptions as recent as 2.8 Ma [Paduan *et al.*, 2009; Davis *et al.*, 2010]; thus, our images may be showing thermal or chemical signatures of mantle upwelling of this age. The low-velocity anomaly is located laterally where mantle lithosphere is expected to thin between the Outer Borderland and Pacific oceanic plate to the west. Our images suggest a mantle lithosphere thickness,

inferred from the seismic wave speeds, of at least 70 km below the region adjacent to and west of the Patton Escarpment as well as below the Outer Borderland and 60 km below the Pacific Plate. The presence of small-scale mantle flow may be producing heterogeneous crustal and mantle lithospheric thicknesses below both oceanic and continental tectonic regimes.

We propose that the ~50 km wide (laterally) region west of the fossil subduction zone (Patton Escarpment) can be described as a thickened lithospheric bulge of slower material, related to the same remnant upwelling asthenosphere responsible for the seamounts described above. While near-surface geology, magnetic anomalies, and bathymetry indicate that the relatively sharp Patton Escarpment relates to ancient subduction, the deeper structure currently present does not directly resemble a subduction zone. For example, this is not part of the accretionary prism lying adjacent to the bulge since the prism's western boundary is marked by the Patton Escarpment. Upwelling magma may be ponding at the base of the crust, resulting in thickening and ongoing adjustment of the lithosphere due to the localized loading. Ongoing cooling and accreting to the underside of the crust could explain an environment enabling the occurrence of deep earthquakes south of the study area but within a similarly narrow band west of the fossil subduction zone [Hauksson *et al.*, 2013]. Anomalously thick oceanic crust and mantle lithosphere has also been observed in a receiver function study using the same OBS data set [Reeves *et al.*, 2015]. From the spatial correlation of this thicker crust with the seamounts and Patton Escarpment (low-velocity anomaly west of the Patton Escarpment in cross sections C-C' and D-D'), we believe that the deeper structure of this transition from oceanic lithosphere to the Continental Borderland is defined by such upwelling rather than ancient subduction.

The new velocity model presented here provides the first complete view of the deeper seismic structure offshore Southern California. It provides a basis for future inversions and modeling with joint data sets, as well as a framework for earthquake locations and ground-shaking simulations for assessing risk associated with offshore faults. It suggests a number of implications regarding the region's tectonic history: The region marking the transition from continental to oceanic crust across the Patton Escarpment is surprisingly diffuse over small length scales and marked by upwelling associated with spreading center volcanism. It also suggests that lithospheric-scale structure under the thinned Inner Borderland has equilibrated since the time of rotation of the Western Transverse Ranges.

Acknowledgments

The authors thank Fan-Chi Lin for assistance with the initial signal processing, tilt and DPG corrections, and dispersion measurements; Yiran Ma for assistance with the 2-D inversions; and Rob Clayton, Asaf Inbal, Joann Stock, Simon Klemperer, and Sampath Rathnayaka for helpful discussions. The final model is available by contacting the corresponding author at dbowden@caltech.edu. SCSN data were provided by the Caltech/USGS Southern California Seismic Network at <http://scedc.caltech.edu/> [California Institute of Technology, Caltech, 1926]. The OBS and DPG waveform data from the ALBACORE array are available from the IRIS Data Management Center at <http://www.iris.edu/hq/>. The IRIS Data Management System is funded through the National Science Foundation and specifically the GEO Directorate through the Instrumentation and Facilities Program of the National Science Foundation under Cooperative Agreement EAR-1063471. The OBS deployment was made possible with instruments and logistical support of the U.S. National Ocean Bottom Seismic Instrumentation Pool (OBSIP) at Scripps Institute of Oceanography; in particular, thanks go to Jeff Babcock, Ernie Aaron, Phil Thai, and Mark Gibaud. The OBS deployment and recovery cruises were made possible with the equipment and logistical support of the University-National Oceanographic Laboratory System (UNOLS) vessel fleet and staff support at Scripps with particular thanks to Jon Meyer, Brian Rowe, and Meghan Donohue. Kohler and Weeraratne thank Captain Curl and the crew of R/V *Melville* for assistance during the 2010 OBS deployment cruise and Captain Vullo and the crew of R/V *New Horizon* during the 2011 OBS recovery cruise. This work was supported by the National Science Foundation (grant OCE-0825254) and by USGS grant G14AP00074.

References

- Atwater, T. (1970), Implications of plate tectonics for the Cenozoic tectonic evolution of Western North America, *Geol. Soc. Am. Bull.*, *81*, 3513–3536.
- Atwater, T. (1989), Plate tectonic history of the northeast Pacific and western North America, The Eastern Pacific ocean and Hawaii, *Geol. Soc. of Am.*, *The Geology of North America*, v. N, 21–72.
- Atwater, T., and J. Stock (1998), Pacific-North America Plate Tectonics of the Neogene Southwestern United States: An update, *Int. Geol. Rev.*, *40*(5), 375–402, doi:10.1080/00206819809465216.
- Barmin, M. P., M. H. Ritzwoller, and A. L. Levshin (2001), A fast and reliable method for surface wave tomography, *Pure Appl. Geophys.*, *158*(8), 1351–1375, doi:10.1007/PL00001225.
- Bell, S. W., D. W. Forsyth, and Y. Ruan (2015), Removing noise from the vertical component records of ocean-bottom seismometers: Results from year one of the Cascadia initiative, *Bull. Seismol. Soc. Am.*, *105*(1), 300–313, doi:10.1785/0120140054.
- Bensen, G. D., M. H. Ritzwoller, M. P. Barmin, A. L. Levshin, F. Lin, M. P. Moschetti, N. M. Shapiro, and Y. Yang (2007), Processing seismic ambient noise data to obtain reliable broad-band surface wave dispersion measurements, *Geophys. J. Int.*, *169*(3), 1239–1260, doi:10.1111/j.1365-246X.2007.03374.x.
- Bohannon, R. G., and E. Geist (1998), Upper crustal structure and Neogene tectonic development of the California continental borderland, *Geol. Soc. Am. Bull.*, *110*(6), 779–800, doi:10.1130/0016-7606(1998)110<0779:UCSANT>2.3.CO;2.
- Bohannon, R. G., and T. Parsons (1995), Tectonic implications of post-30 Ma Pacific and North American relative plate motions, *Geol. Soc. Am. Bull.*, *107*(8), 937–959, doi:10.1130/0016-7606(1995)107<0937:TIOIMP>2.3.CO;2.
- California Institute of Technology (Caltech) (1926), Southern California Seismic Network, International Federation of Digital Seismograph Networks. Other/Seismic Network, doi:10.7914/SN/CI.
- Crawford, W. C., and S. C. Webb (2000), Identifying and removing tilt noise from low frequency LT0.1 Hz seafloor vertical seismic data, *Bull. Seismol. Soc. Am.*, *90*(4), 952–963.
- Crouch, J. K., and J. Suppe (1993), Late Cenozoic tectonic evolution of the Los-Angeles Basin and Inner California Borderland—A model for core complex like crustal extension, *Geol. Soc. Am. Bull.*, *105*(11), 1415–1434, doi:10.1130/0016-7606(1993)105<1415:LCTEOT>2.3.CO;2.
- Crowell, J. C. (1968), Movement histories of faults in the Transverse ranges and speculations on the tectonic history of California, in *Proceedings of the Conference on Geologic Problems of the San Andreas Fault System*, *Publ. Geol. Sci.*, vol. 11, edited by W. R. Dickinson and A. Grantz, pp. 323–341, Stanford Univ. Publ. Geol. Sci., Palo Alto, Calif.
- Davis, A. S., D. A. Clague, J. B. Paduan, B. L. Cousins, and J. Huard (2010), Origin of volcanic seamounts at the continental margin of California related to changes in plate margins, *Geochem. Geophys. Geosyst.*, *11*, Q05006, doi:10.1029/2010GC003064.
- Dokka, R. K. (1989), The Mojave extensional belt of Southern California, *Tectonics*, *8*, 363–390, doi:10.1029/TC008i002p00363.
- Feigl, K. L., et al. (1993), Space geodetic measurement of crustal deformation in central and Southern California, 1984–1992, *J. Geophys. Res.*, *98*(B12), 21,677–21,712, doi:10.1029/93JB02405.
- Fuis, G. S. (1998), West margin of North America—A synthesis of recent seismic transects, *Tectonophysics*, *288*(1–4), 265–292, doi:10.1016/S0040-1951(97)00300-4.
- Fuis, G. S., et al. (2003), Fault systems of the 1971 San Fernando and 1994 Northridge earthquakes, Southern California: Relocated aftershocks and seismic images from LARSE II, *Geology*, *31*(2), 171–174, doi:10.1130/0091-7613(2003)031<0171:FSOTSF>2.0.CO;2.
- Fuis, G. S., D. S. Scheirer, V. E. Langenheim, and M. D. Kohler (2012), A new perspective on the geometry of the San Andreas fault in Southern California and its relationship to lithospheric structure, *Bull. Seismol. Soc. Am.*, *102*(1), 236–251, doi:10.1785/0120110041.

- Gao, H., and Y. Shen (2015), A preliminary full-wave ambient-noise tomography model spanning from the Juan de Fuca and Gorda spreading centers to the Cascadia volcanic arc, *Seismol. Res. Lett.*, *86*(5), 1253–1260, doi:10.1785/0220150103.
- Gimbert, F., and V. C. Tsai (2015), Predicting short-period, wind-wave-generated seismic noise in coastal regions, *Earth Planet. Sci. Lett.*, *426*, 280–292, doi:10.1016/j.epsl.2015.06.017.
- Hadley, D., and H. Kanamori (1977), Seismic structure of the Transverse Ranges, California, *Geol. Soc. Am. Bull.*, *88*(10), 1469–1478, doi:10.1130/0016-7606(1977)88<1469:SSOTTR>2.0.CO;2.
- Harmon, N., D. Forsyth, and S. Webb (2007), Using ambient seismic noise to determine short-period phase velocities and shallow shear velocities in young oceanic lithosphere, *Bull. Seismol. Soc. Am.*, *97*(6), 2009–2023, doi:10.1785/0120070050.
- Hauksson, E., H. Kanamori, J. Stock, M.-H. Cormier, and M. Legg (2013), Fracturing the eastern edge of the Pacific Ocean lithosphere as evidenced by seismicity in the abyssal plain off Baja California, Mexico, *Geophys. J. Int.*, doi:10.1093/gji/gg1467.
- Herrmann, R. B. (2013), Computer programs in seismology: An evolving tool for instruction and research, *Seismol. Res. Lett.*, *84*(6), 1081–1088, doi:10.1785/0220110096.
- Humphreys, E., and R. Clayton (1990), Tomographic image of the southern California mantle, *J. Geophys. Res.*, *95*(B12), 19,725–19,746, doi:10.1029/JB095iB12p19725.
- Klemperer, S. L., T. A. Hauge, E. C. Hauser, J. E. Oliver, and C. J. Potter (1986), The Moho in the northern Basin and Range province, Nevada, along the COCORP 40 N seismic-reflection transect, *Geol. Soc. Am. Bull.*, *97*(5), 603–618.
- Kohler, M. D. (1999), Lithospheric deformation beneath the San Gabriel Mountains in the southern California Transverse Ranges, *J. Geophys. Res.*, *104*(B7), 15,025–15,041, doi:10.1029/1999JB900141.
- Kohler, M. D., H. Magistrale, and R. W. Clayton (2003), Mantle heterogeneities and the SCEC reference three-dimensional seismic velocity model version 3, *Bull. Seismol. Soc. Am.*, *93*(2), 757–774, doi:10.1785/0120020017.
- Kohler, M., K. Booth, C. Sun, C. Curl, C. Finnell, P. Shute, W. B. Prine, J. Ramos, and W. Brown (2010), ALBACORE OBS Deployment Cruise Report, R/V Melville Cruise MV1010, 27 pp., 14–27 Aug. 2010.
- Kohler, M., K. Brunner, M. Donohue, D. Weaver, T. Chi, and M. Breen (2011), ALBACORE OBS Recovery Cruise Report, R/V New Horizons Cruise NH1111, 35 pp., 7–16 Sept. 2011.
- Legg, M. R. (1991), Developments in understanding the tectonic evolution of the California Continental Borderland, in *From Shoreline to Abyss*, vol. 46, edited by R. H. Osborne, pp. 291–312, SEPM Shepard Commemorative, Tulsa, Okla.
- Legg, M. R., M. D. Kohler, N. Shintaku, and D. S. Weeraratne (2015), High-resolution mapping of two large-scale transpressional fault zones in the California Continental Borderland: Santa Cruz-Catalina Ridge and Ferrello faults, *J. Geophys. Res. Earth Surf.*, *120*, 915–942, doi:10.1002/2014JF003322.
- Levshin, A. L., and M. H. Ritzwoller (2001), Automated detection, extraction, and measurement of regional surface waves, *Pure Appl. Geophys.*, *158*(8), 1531–1545, doi:10.1007/978-3-0348-8264-4_11.
- Lin, F. C., M. H. Ritzwoller, and N. M. Shapiro (2006), Is ambient noise tomography across ocean basins possible?, *Geophys. Res. Lett.*, *33*, L14304, doi:10.1029/2006GL026610.
- Longuet-Higgins, M. S. (1950), A theory of the origin of microseisms, *Philos. Trans. R. Soc., A*, *243*(857), 1–35, doi:10.1098/rsta.1979.0079.
- Lonsdale, P. (1991), Structural patterns of the Pacific floor offshore of Peninsular California, in *The Gulf and Peninsular Province of the Californias*, AAPG Mem., vol. 47, chap. 7, edited by J. P. Dauphin and B. R. T. Simoneit, pp. 87–125, Am. Assoc. Petrol. Geol., Tulsa, Okla.
- Loris, I., G. Nolet, I. Daubechies, and F. A. Dahlen (2007), Tomographic inversion using ℓ_1 -norm regularization of wavelet coefficients, *Geophys. J. Int.*, *170*(1), 359–370.
- Luyendyk, B. P. (1991), A model for Neogene crustal rotations, transtension, and transpression in Southern California, *Geol. Soc. Am. Bull.*, *103*, 1528–1536.
- Ma, Y., and R. W. Clayton (2014), The crust and uppermost mantle structure of Southern Peru from ambient noise and earthquake surface wave analysis, *Earth Planet. Sci. Lett.*, *395*, 61–70, doi:10.1016/j.epsl.2014.03.013.
- Miller, K. (2002), Geophysical evidence for Miocene extension and mafic magmatic addition in the California Continental Borderland, *Geol. Soc. Am. Bull.*, *114*(4), 497–512, doi:10.1130/0016-7606(2002)114<0497:GEFMEA>2.0.CO;2.
- Nazareth, J. J., and R. W. Clayton (2003), Crustal structure of the Borderland-Continent transition zone of Southern California adjacent to Los Angeles, *J. Geophys. Res.*, *108*(B8), 2404, doi:10.1029/2001JB000223.
- Nicholson, C., C. C. Sorlien, T. Atwater, J. C. Crowell, and B. P. Luyendyk (1994), Microplate capture, rotation of the western Transverse Ranges, and initiation of the San Andreas transform as a low-angle fault system, *Geology*, *22*(6), 491–495, doi:10.1130/0091-7613(1994)022<0491:MCROTW>2.3.CO;2.
- Paduan, J. B., D. A. Clague, and A. S. Davis (2009), Evidence that three seamounts off Southern California were ancient islands, *Mar. Geol.*, *265*(3–4), 146–156, doi:10.1016/j.margeo.2009.07.003.
- Parsons, T. (1995), The basin and range province, *Cont. Rifts: Evol. Struct. Tecton.*, *25*, 277–324.
- Raikes, S. A. (1980), Regional variations in upper mantle structure beneath Southern California, *Geophys. J. R. Astron. Soc.*, *63*, 187–216.
- Reeves, Z., V. Lekić, N. Schmerr, M. Kohler, and D. Weeraratne (2015), Lithospheric structure across the California Continental Borderland from receiver functions, *Geochem. Geophys. Geosyst.*, *16*, 246–266, doi:10.1002/2014GC005617.
- Romanyuk, T., W. D. Mooney, and S. Detweiler (2007), Two lithospheric profiles across Southern California derived from gravity and seismic data, *J. Geodyn.*, *43*(2), 274–307, doi:10.1016/j.jog.2006.09.011.
- Shaw, J. H., et al. (2015), Unified structural representation of the Southern California crust and upper mantle, *Earth Planet. Sci. Lett.*, *415*, 1–15, doi:10.1016/j.epsl.2015.01.016.
- Shen, Z., D. D. Jackson, and B. X. Ge (1996), Crustal deformation across and beyond the Los Angeles basin from geodetic measurements, *J. Geophys. Res.*, *101*, 27, 957–27, 980, doi:10.1029/96JB02544.
- Stock, J. M., and K. V. Hodges (1989), Pre-Pliocene extension around the Gulf of California and the transfer of Baja California to the Pacific plate, *Tectonics*, *8*, 99–115, doi:10.1029/TC008i001p00099.
- ten Brink, U. S., J. Zhang, T. M. Brocher, D. A. Okaya, K. D. Klitgord, and G. S. Fuis (2000), Geophysical evidence for the evolution of the California Inner Continental Borderland as a metamorphic core complex, *J. Geophys. Res.*, *105*(1999), 5835–5857, doi:10.1029/1999JB900318.
- Tennyson, M. E. (1989), Pre-transform early Miocene extension in western California, *Geology*, *17*, 792–796.
- Vedder, J. G., L. A. Beyer, A. Junger, G. W. Moore, A. E. Roberts, J. C. Taylor, and H. C. Wagner (1974), Preliminary report on the geology of the continental borderland of Southern California, 264.
- Walck, M. C., and J. B. Minster (1982), Relative array analysis of upper mantle lateral velocity variations in Southern California, *J. Geophys. Res.*, *87*, 1757–1772, doi:10.1029/JB087iB03p01757.
- Walls, C., T. Rockwell, K. Mueller, Y. Bock, S. Williams, J. Pfanner, J. Dolan, and P. Fang (1998), Escape tectonics in the Los Angeles metropolitan region and implications for seismic risk, *Nature*, *394*, 356–360.

- Webb, S. C. (1998), Broadband seismology and noise under the ocean, *Rev. Geophys.*, 36(1), 105–142, doi:10.1029/97RG02287.
- Webb, S. C., and W. C. Crawford (1999), Long-period seafloor seismology and deformation under ocean waves, *Bull. Seismol. Soc. Am.*, 89(6), 1535–1542.
- Weigand, P. W. (1994), Petrology and geochemistry of Miocene volcanic rocks from Santa Catalina and San Clemente Islands, California, in *Proceedings of the Fourth California Island Symposium*, edited by W. L. Halvorson and G. J. Maender, pp. 267–280, Santa Barbara Museum of Natural History, Santa Barbara, Calif.
- Wright, T. L. (1991), Structural geology and tectonic evolution of the Los Angeles basin, California, in *Active Margin Basins, AAPG Mem.*, vol. 52, edited by K. T. Biddle, pp. 35–134, Am. Assoc. Petrol. Geol., Tulsa, Okla.
- Yao, H., P. Gouédard, J. A. Collins, J. J. McGuire, and R. D. van der Hilst (2011), Structure of young East Pacific Rise lithosphere from ambient noise correlation analysis of fundamental- and higher-mode Scholte-Rayleigh waves, *C. R. Geosci.*, 343(8-9), 571–583, doi:10.1016/j.crte.2011.04.004.